ICAS 2021 SHANG HAI
International Council of the Aeronautical Sciences
32nd Congress of the International Council of the Aeronautical Sciences
September 6-10, 2021
Pudong Shangri-La, Shanghai, China

A LOCAL CORRELATION-BASED ALGEBRAIC TRANSITION MODEL WITH COMPRESSIBILITY AND CROSSFLOW CORRECTION

Ruixuan Xie[1], Weimin Sang[1]

[1]School of Aeronautics, Northwestern Polytechnical University, Xi'an 710072, People's Republic of China

Abstract

LCTMs are now commonly used in RANS solvers for predicting laminar-turbulent transition. In 2020, an algebraic LCTM called BCM was proposed. Results of the BCM model exhibit good agreements with experiments and predictions from other one- or two-equation LCTMs in low-speed, two-dimensional flow. However, this model did not include the effect of compressibility and crossflow, making it less accurate in handling transonic and swept-wing problems. In this paper, without adding extra equations, the compressibility and crossflow corrections are integrated into the BCM to form a new model called BCMcc. Next, the crossflow term is calibrated using a 6:1 inclined spheroid. Then the new model and other LCTMs were used to predict the transition on the DLR-F4 and CRM-NLF aircraft. Compared to the BCM model and some other more complex models, the BCMcc model's predictions are more consistent with experimental results in transonic and crossflow conditions, meaning it can be useful for transition prediction in the NLF design of future aircraft.

Keywords: transition model, turbulence model, natural laminar flow

1. Introduction

The change of flow from laminar to turbulent is known as transition. On the surface of modern transonic aircraft, the transition starts quickly at the nose and leading edges. The turbulent boundary layer after transition creates drag five to ten times greater than the laminar boundary layer and accounts for half of the total [1]. Therefore, natural laminar flow (NLF) and laminar flow control (LFC) technology that can delay the transition and drastically reduce drag is attractive. Using such technology requires the computational fluid dynamics (CFD) solver to predict the transition induced by the growth and eventually breakdown of several kinds of waves. On aircraft surfaces, those are mainly Tollmien-Schlichting (TS) waves and crossflow (CF) waves.

The e^N method [2][3] that calculates the growth of waves along streamlines, and determines transition when the wave exceeds a certain level, was applied to many engineering applications successfully. But its numerous non-local operations are difficult to fit in modern parallel Reynolds average Navier-Stokes (RANS) solvers [4]. Local correlation-based transition models (LCTMs) are more preferable, which do not compute how waves amplify but rely entirely on the empirical correlations between transition and local variables. Most LCTMs are in the form of transport equations similar to the turbulence models they cooperate with, and can therefore be easily integrated into existing codes. In 2004, Menter et al. proposed the famous γ-Re_θ model [5] consisting of two transport equations, one for an intermittency factor γ and the other for a Reynolds number $Re_{\theta t}$. Coupled with the two-equation SST turbulence model, the γ-Re_θ model can accurately predict the transition induced by TS waves, high turbulent intensity, and flow separation. The model shows good versatility and is used for a wide range of flows from internal to external, but the need for solving 4 partial differential equations (PDEs) simultaneously caused more complexity and computing costs. To reduce the number of transport equations, in 2015 Menter et al. created a one-equation γ model by replacing the $Re_{\theta t}$ equation in the γ-Re_θ model with empirical functions [6]. A more progressive approach was made by Bas and Cakmakcioglu as they proposed an algebraic LCTM called BC in 2013 [7], which was later modified into a Galilean invariant form called BCM in 2020 [8]. Instead of transport equations, only algebraic functions are used to compute the intermittency factor. While predicting TS wave-induced transition in incompressible flows accurately [8][9], the algebraic model

is easier to implement. Only two coefficients are contained, meaning it could be fastly calibrated for different problems. Additionally, It was reported 37% faster than the one-equation γ model [10] and achieved a 24% time and 15% memory saving when combined with delay detached eddy simulation, compared to the γ-Re_θ model [11]. However, on the surface of a swept-wing transonic aircraft, the transition on the inboard wing is usually dominated by CF waves [12], and TS waves on the outboard wing are significantly stabilized due to the increased compressibility of air [13]. The absence of these two effects in the BCM model leads to overestimated laminar regions on the inboard wing and underestimated ones on the outboard. The BCM model also uses freestream turbulent intensity instead of local turbulent intensity, which limits its application to external flows.

When focusing on only one type of problem, non-generic models that can be easily calibrated and programmed are also valuable and have the potential to achieve higher accuracy when properly calibrated. In this paper, a compressibility correction computed from the local Mach number is proposed and a crossflow correction from Javadi [10], which is originally designed for the BC model, is simplified and calibrated. These two corrections are then integrated into the BCM model to predict the transition on DLR-F4 and CRM-NLF transonic aircraft. Results are compared with relevant experiments together with computations from other LCTMs.

2. Model formulation

2.1 The BCM model

The SA turbulence model that the BCM model is based on is given by:

$$\frac{\partial \tilde{\nu}}{\partial t} + u_j \frac{\partial \tilde{\nu}}{\partial x_j} = C_{b1} S \tilde{\nu} - C_{w1} f_w \left(\frac{\tilde{\nu}}{d}\right)^2 + \frac{1}{\sigma}\left\{\frac{\partial}{\partial x_j}\left[(\nu_L + \tilde{\nu})\frac{\partial \tilde{\nu}}{\partial x_j}\right] + C_{b2}\frac{\partial \tilde{\nu}}{\partial x_j}\frac{\partial \tilde{\nu}}{\partial x_j}\right\} \tag{1}$$

And the turbulent viscosity μ_T is computed from:

$$\mu_T = \rho \tilde{\nu} f_{\nu 1}$$

where

$$f_{\nu 1} = \frac{\chi^3}{\chi^3 + c_{\nu 1}^3}, \chi^3 = \frac{\tilde{\nu}}{\nu}, c_{\nu 1} = 7.1 \tag{2}$$

and ρ is the density, ν is the molecular kinematic viscosity. We focus on the production term located in the first term on the right-hand side of equation (1). The BCM model uses an intermittency function γ_{BC} multiplying with the production term to control the production of the $\tilde{\nu}$ and thus the μ_T:

$$\gamma_{BC} C_{b1} S \tilde{\nu} \tag{3}$$

The intermittency function is given as in the followings

$$\gamma_{BC} = 1 - \mathrm{e}^{\left(-\sqrt{Term_1} - \sqrt{Term_2}\right)} \tag{4}$$

$$Term_1 = \frac{max(Re_\theta - Re_{\theta t}, 0.0)}{\chi_1 Re_{\theta t}} \tag{5}$$

$$Term_2 = max\left(\frac{1}{\chi_2}\frac{\mu_T}{\mu}, 0.0\right) \tag{6}$$

$$Re_\theta = \frac{Re_\nu}{2.193} \tag{7}$$

$$Re_\nu = \frac{\rho d_w^2}{\mu}\Omega \tag{8}$$

$$Re_{\theta t} = 803.73(Tu_\infty + 0.6067)^{-1.027} \tag{9}$$

where $\chi_1 = 0.002$, $\chi_2 = 0.02$, Re_θ is the momentum thickness Reynolds number, $Re_{\theta t}$ is the Re_θ where the transition onsets, Tu_∞ is the freestream turbulent intensity, d_w is the distance from the nearest wall, and Ω is the vorticity magnitude. Equation (9) is the correlation between the $Re_{\theta t}$ and Tu_∞ acquired from experiments. However, computation of the Re_θ needs integration of the boundary-layer velocity profile in non-local cells. To achieve a fully localized solution, the BCM model uses (7) to relate the Re_θ with the locally computed vorticity Reynolds number Re_ν. Such an idea is based on Van Driest and Blumer's observation [14] and is also adopted by the γ-Re_θ model.

Figure 1 shows how γ_{BC}, μ_T/μ, and the ratio of the local Mach number to the Mach number external of the boundary layer Ma/Ma_e varies on a flat plate. In the laminar region, the Re_θ does not exceed the $Re_{\theta t}$, therefore $Term_1$ equals zero. At the same time, $Term_2$ remains very small due to the near-zero μ_T in the laminar flow region. Resulting in a near-zero γ_{BC} and so damps the production of μ_T. Once the Re_θ exceeds the $Re_{\theta t}$, $Term_1$ and γ_{BC} will be triggered, allowing the production of μ_T. As in (8), Re_v is proportional to d_w^2, which means it is a small value near the wall and no μ_T could produce if using $Term_1$ solely. Therefore, another term is needed to transport the information of transition onset to the bottom of the boundary layer. Instead of deriving extra transport equations, the BCM model uses the already transported μ_T. The $Term_2$ checks if enough μ_T has been generated, if so, it would burst and transport the turbulence to the entire boundary layer downstream to complete the transition. Flow downstream would be determined fully turbulent as γ_{BC} approaches 1 and the turbulence model recovers to the original SA model.

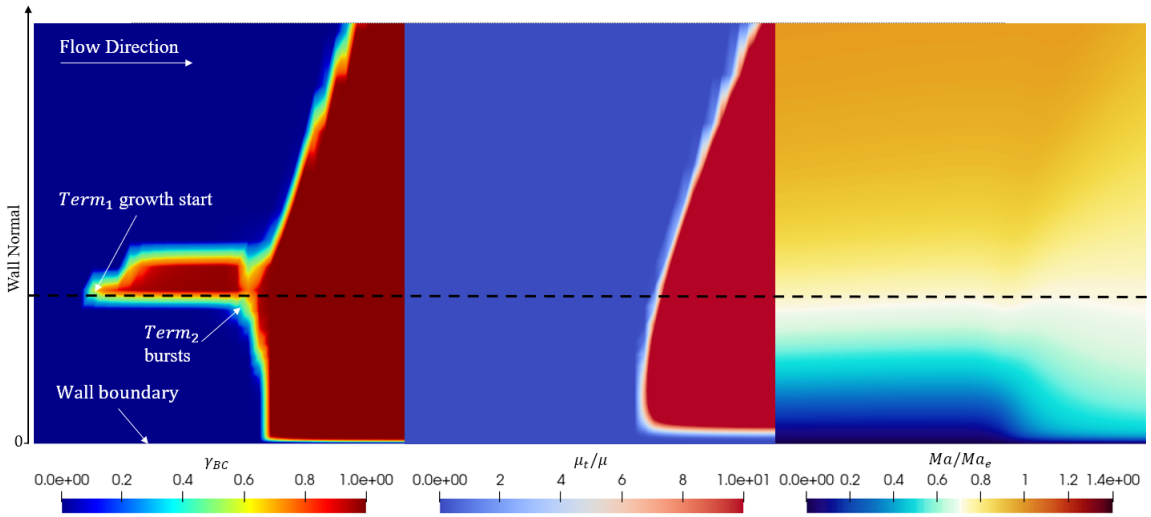

Figure 1 – Contours of γ_{BC}, μ_T/μ, and Ma/Ma_e on a flat plate.

2.2 Compressibility correction

The original BCM model is calibrated based on the low-speed flat-plate experiment. In compressible flows however, the TS wave is stabilized and the transition Reynolds number Re_x varies with Mach number external of the boundary layer Ma_e, where x is the length of a laminar region. The $Re_x(Ma_e)$ correlation was acquired by applying the e^N method [13] and measuring on an in-flight 10° cone [15]. But a $Ma(Ma_e)$ correlation that holds in the entire boundary layer does not exist as the Ma varies from 0 to Ma_e with wall distance. As in Figure 1, we observed that the $Term_1$ starts growing at a wall normal position where $Ma \approx 0.7Ma_e$. Assuming that such relation is a good approximation for all other cases, a compressibility function $G(Ma)$ could be written as follow:

$$G(Ma) = Re_x(Ma)/Re_x(0) = 3.55/[1.0 + (Ma/0.76)^{-3.33}] + 1.0 \quad (10)$$

Figure 2 shows the $G(Ma)$ computed from the data of [13], [15], and (10), all assuming $Ma = 0.7Ma_e$. At $Ma \in [0,1.6]$or$Ma_e \in [0,2.3]$, the curve of present correlation fits the e^N method's calculation and measurements.

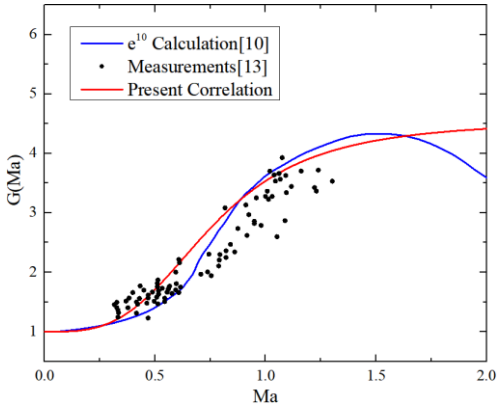

Figure 2 – Computed and measured $G(Ma)$

In a Blasius boundary layer before transition, θ is proportional to $\sqrt{x}$, thus $\sqrt{G(Ma)}$ is then multiplied with the uncorrected $Re_{\theta t}$ in (8) to provide the corrected $Re_{\theta t,c}$ for $Term_1$ calculation.

$$Re_{\theta t,c} = \sqrt{G(Ma)}803.73(Tu_\infty + 0.6067)^{-1.027} \tag{11}$$

2.3 Crossflow correction

In a three-dimensional flow, for example on a swept wing, crosswise pressure gradients induce an inflection point and crossflow component in the boundary layer velocity profile and lead to an accelerated transition [16]. For prediction of the crossflow transition, Arnal et al. proposed an experimental correlation called 'C1 criteria' [17] which is given by:

$$\frac{Re^*_{\delta 2t}}{Re^*_{\delta 2t,tr}} \geq 1 \tag{12}$$

where $Re^*_{\delta 2t}$ is the crossflow displacement thickness Reynolds number and $Re^*_{\delta 2t,tr}$ is the critical Reynolds number. When the $Re^*_{\delta 2t}$ exceeds the $Re^*_{\delta 2t,tr}$, crossflow transition is triggered. The $Re^*_{\delta 2t,tr}$ is a function of the boundary layer shape factor H as defined below:

$$Re^*_{\delta 2t,tr} = \begin{cases} \dfrac{300}{\pi} arctan\left[\dfrac{0.106}{(H-2.3)^{2.052}}\right], & 2.3 < x \leq 2.7 \\ 150 \quad , & x \leq 2.3 \end{cases} \tag{13}$$

The new parameter H is unfavorable since it requires wall-normal vectors that are not used in the BCM model. But It appears that a constant $Re^*_{\delta 2t,tr} = 150$ is not a bad approximation. According to [10], the $Re^*_{\delta 2t}$ is computed as follow:

$$Re^*_{\delta 2t} = C_{cf}\Delta H_{cf} Re_{\theta t} \tag{14}$$

$$\Delta H_{cf} = \frac{|\zeta| d_w}{|\vec{u}|^2}\left[1.0 + min\left(\frac{\mu_T}{\mu}, 0.4\right)\right] \tag{15}$$

$$\zeta = (\nabla \times \vec{u}) \cdot \vec{u} \tag{16}$$

where C_{cf} is a coefficient that needs calibration, ζ is the helicity introduced by Langtry et al. as a measure of the crossflow strength [18]. The $Re_{\theta t}$ is the uncorrected Reynolds number given by (8) as the CF wave is not sensitive to compressibility [13]. γ_{BC} is limited to zero where $\rho > 1.05\rho_\infty$ to prevent early transition at leading edges. The complete BCM model with compressibility and crossflow correction (herein referred to as 'BCMcc') reads:

$$\gamma_{BC} = \begin{cases} 1 - \mathrm{e}^{\left(-\sqrt{Term_1}-\sqrt{Term_4}\right)}, & \rho \leq 1.05\rho_\infty \\ 0, & \rho > 1.05\rho_\infty \end{cases} \tag{17}$$

$$Term_1 = \frac{max\left(Re_\theta - Re_{\theta t,c},\ 0.0\right)}{\chi_1 Re_{\theta t,c}} \tag{18}$$

$$Term_2 = max\left(\frac{1}{\chi_2}\frac{\mu_T}{\mu},\ 0.0\right) \tag{6}$$

$$Term_3 = min\left[max\left(\frac{Re^*_{\delta 2t}}{150} - 1.0,\ 0.0\right),\ 1.0\right] \tag{19}$$

$$Term_4 = max(Term_2, Term_3) \tag{20}$$

2.4 Flow solvers and numerical Methods

The BCMcc model is implemented in the open-sourced Stanford University Unstructured (SU2) CFD platform [19]. The comprehensive program structure and variable naming of SU2 enable simple programming. The JST and the first-order upwind schemes are used to calculate the convective fluxes in the flow and turbulence equations respectively. To evaluate the viscous fluxes, flow quantities and their first derivatives are required at the faces of the control volumes. The gradients of the flow variables are calculated using either a Green–Gauss method at all grid nodes. Besides, the Fluent code is used to solve the γ-Re_θ and γ cases, with Roe and second-order upwind schemes for convective fluxes, and Grenn-Gauss node-based method for gradients. Both solvers use the implicit Euler method to converge the problem.

3. Calibration and validation

3.1 6:1 inclined prolate spheroid

The 6:1 inclined prolate spheroid geometry produces strong crossflow that is challenging to LCTMs, so it is chosen for the calibration of the C_{cf}. The experiment [20] was conducted in the low-speed wind tunnel at the DFVLR Göttingen with an angle of attack $\alpha = 15°$, $Tu_\infty = 0.2\%$, freestream Mach number $Ma_\infty = 0.136$ and $Re_c = 6.5 \times 10^6$ based on the length of the spheroid. The result from the γ-Re_θ and γ model (with crossflow effect included) are also plotted for comparison. Figure 3 shows the half model mesh with 5.85 million generated for computation.

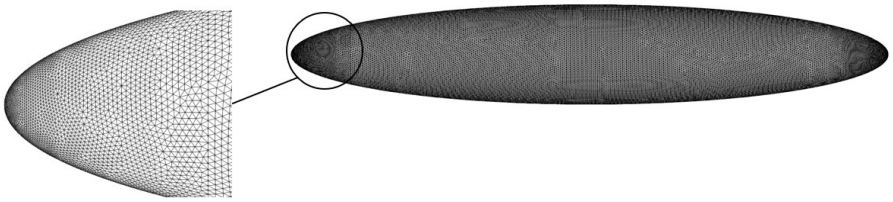

Figure 3 – Surface mesh of the 6:1 inclined prolate spheroid

Rough adjustment of C_{cf} is made to match the area of the laminar region, the result is $C_{cf} = 0.9$. As in Figure 4, both the BCM model and the γ-Re_θ model overpredict the laminar region as they don't solve the CF instability. The γ model shows the effect of crossflow, but the accuracy of the transition front is not optimal. The BCMcc model predicts the transition correctly at the bottom and top of the spheroid, although the laminar area is larger than the experimental at the middle. the result overall is acceptable and better than those of more complex models.

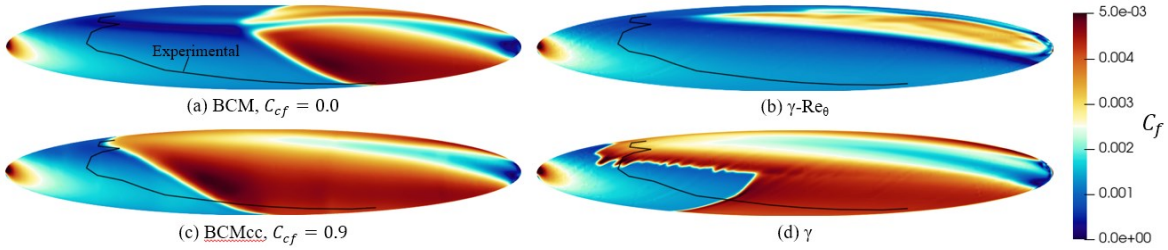

Figure 4 – Skin friction coefficient (C_f) contours on a 6:1 prolate spheroid

3.2 DLR-F4 aircraft

The DLR-F4 is a transonic aircraft geometry proposed during the 1st CFD Drag Prediction Workshop. In 2003, Fey et al. [21] conducted transition measurements in the European Transonic Windtunnel using temperature-sensitive paint (TSP). A constant Reynolds number based on the mean Aerodynamic chord of $Re_{MAC} = 6.0 \times 10^6$, constant Mach number of 0.785 and four angles of attack (α) from -4.85° to -0.87° is tested. The Tu_∞ of the wind tunnel is less than 0.05% and we assume a 0.04% in the following calculations. A hybrid mesh of 18 million cells (half model) is generated and shown in Figure 5. Cells on the upper wing surface are 400×180×50 hexahedrons (spanwise×chordwise×normal). Beyond the region of hexahedrons, cells are tetrahedrons or prisms. The y^+ of the first layer near walls is 0.75 and the growth rate between layers is 1.15. To distinguish between TS wave-induced and CF wave-induced transition, the $Term_3$ in the BCMcc model is removed, forming a model that contains only compressibility correction and no crossflow correction. Such a model is referred to as BCMc. When the BCMc and BCMcc models predict transition differently, it indicates that the transition is induced by crossflows.

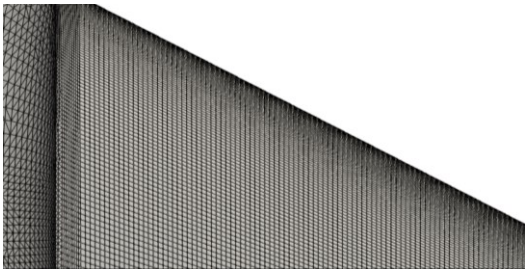

Figure – 5 Mesh on the upper surface of the wing

Figures 6 to 8 are the skin friction coefficient contour computed for $\alpha = -0.87°$, $-1.58°$, and $-2.59°$ respectively, with blue-colored area indicating the laminar flow. The experimental transition fronts according to [21] are drawn as black lines on those fully turbulent pictures. In all 3 conditions, the fully-turbulent model gives no laminar region as expected. The BCM model successfully predicts some of the laminar regions, although the transition is imprecise due to the underestimated $Re_{\theta t,c}$. On the outboard wing where transition is mostly shock-induced, the BCMc and BCMcc model and the experiment all result in straight transition fronts. On the inboard wing and wingtip, the transition fronts from these two models are different, suggesting that the transition is induced by CF waves. Saw-toothed patterns on the inboard wing are also seen in the high-resolution TSP images obtained in the experiment, the authors consider these to be a sign of crossflow transition. We found the common point of these places is the presence of pressure gradients. As in Figure 9, adverse pressure deflects the streamline outwards, inducing strong crossflow and shaping a "stepped" transition front. In $\alpha = -0.87°$ and $-1.58°$ cases early transition fronts are predicted on the inboard wing when using the BCMcc model. These early fronts are not necessarily caused by an inaccurate $Term_3$, but could also be a consequence of differences between the calculated pressure distributions and the experimental ones. In $\alpha = -2.59°$ case all models failed to predict the transition on the inboard wing correctly, with only the BCMcc model yields a reasonable result on the outboard wing. However, according to [21], the lift coefficient in such conditions is 0.3 (designed for 0.5) which is not commonly used. Therefore, the error is tolerable.

Figure 10 shows skin friction distributions computed with the γ-Re$_\theta$ and the γ model. On the inboard section where CF waves dominate the transition, the γ-Re$_\theta$ model overestimates the laminar region as expected. On the outboard section, the exhibited transition front satisfactorily agrees with the experiment. However, the γ model gives almost no laminar region, which significantly differs from the experiment. Reasons for this are pending further research. Overall, both the γ-Reθ model and the BCMcc model perform well in regions dominated by TS waves. However, as the CF waves become stronger, the more difficult it becomes for the γ-Reθ model to give correct results, and the advantages of the BCMcc model begin to emerge.

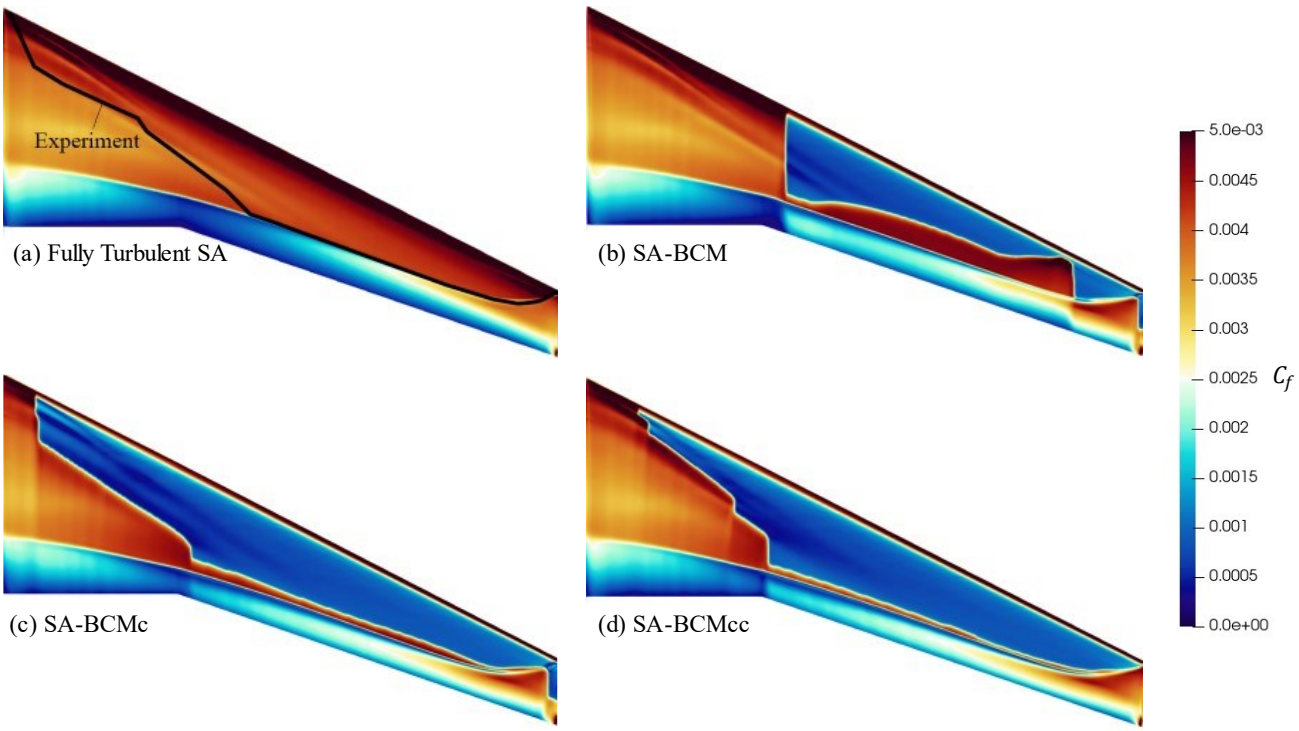

Figure 6 – Experimental transition front and calculated skin friction coefficient on the DLR-F4 wing, $\alpha = -0.87°$, $Ma_\infty = 0.785$, $Re_{MAC} = 6.0 * 10^6$

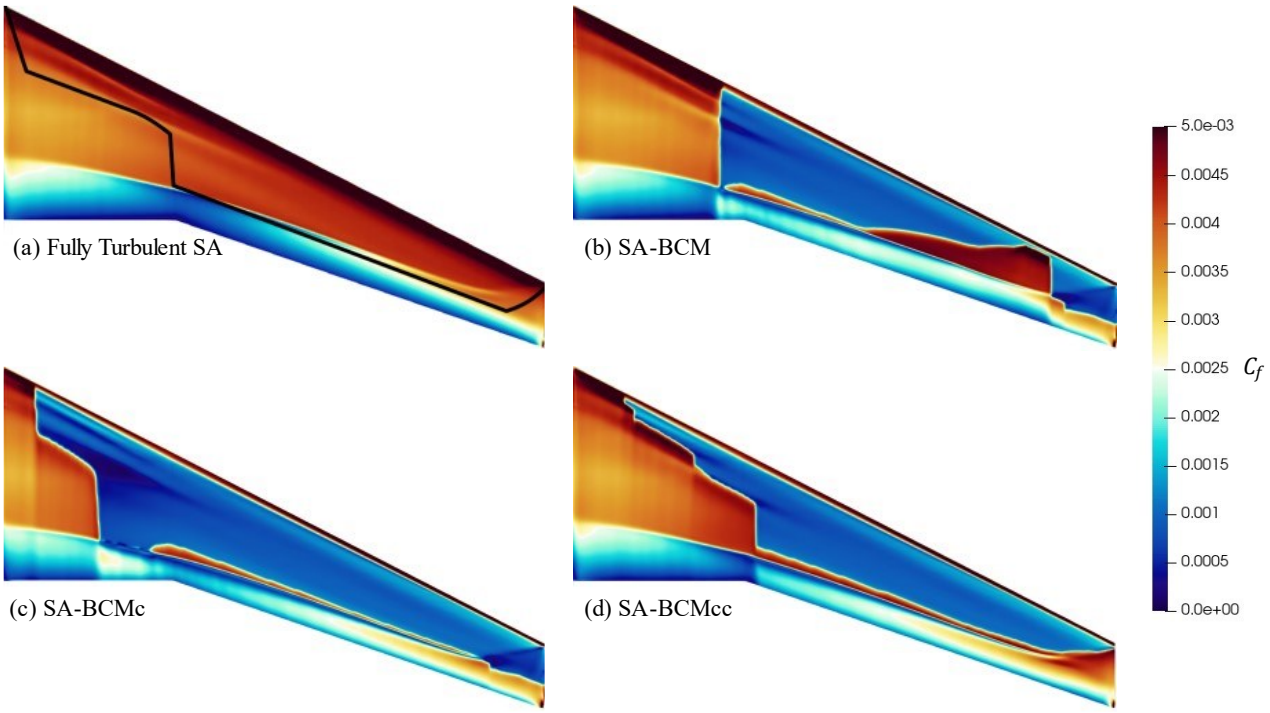

Figure 7 – Experimental transition front and calculated skin friction coefficient on the DLR-F4 wing, $\alpha = -1.58°$, $Ma_\infty = 0.785$, $Re_{MAC} = 6.0 * 10^6$

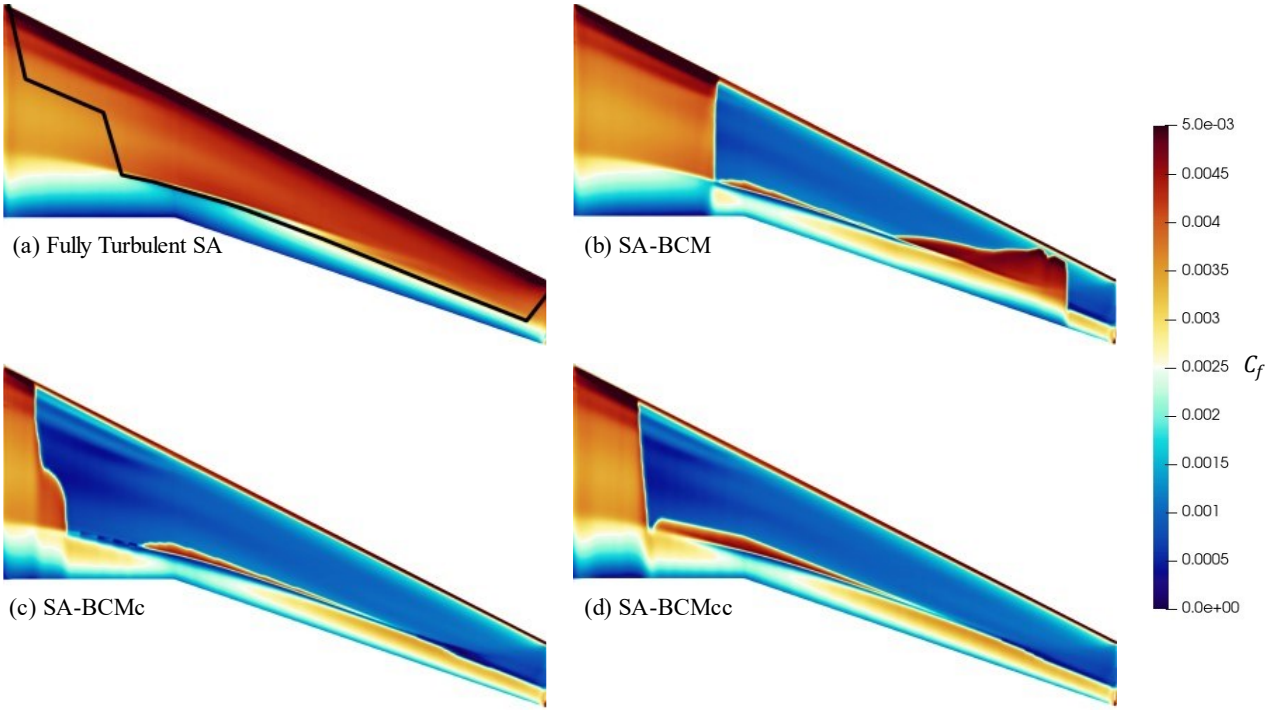

Figure 8 – Experimental transition front and calculated skin friction coefficient on the DLR-F4 wing, $\alpha = -2.59°$, $Ma_\infty = 0.785$, $Re_{MAC} = 6.0 * 10^6$

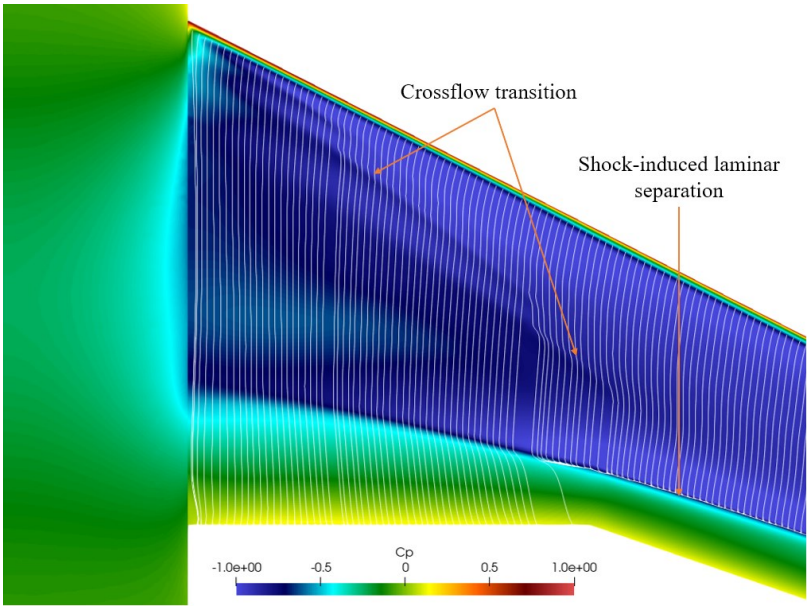

Figure 9 – Computed with BCMcc model, surface streamlines and pressure coefficient contour on the DLR-F4 wing, $\alpha = -0.87°$, $Ma_\infty = 0.785$, $Re_{MAC} = 6.0 * 10^6$

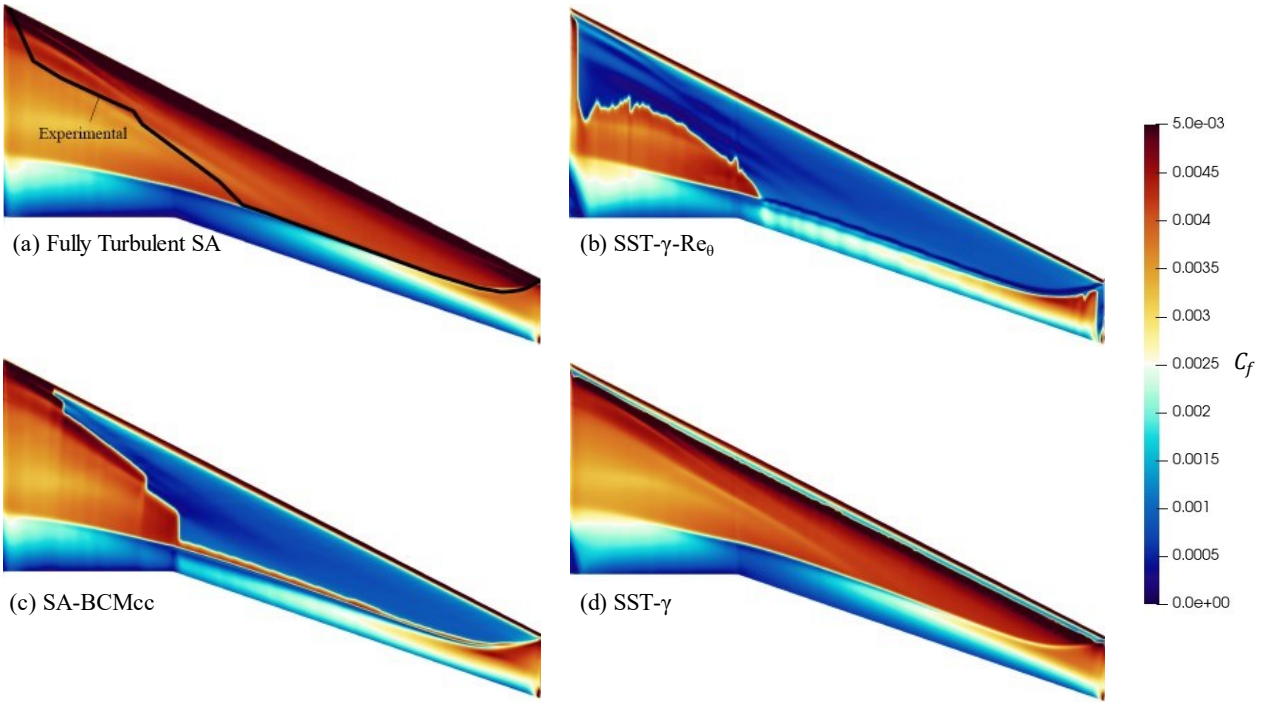

Figure 10 – Skin friction coefficient contour on the DLR-F4 wing computed with 4 different models, $\alpha = -0.87°$, $Ma_\infty = 0.785$, $Re_{MAC} = 6.0 * 10^6$

3.3 CRM-NLF aircraft

The CRM-NLF is a transonic wind tunnel model designed by NASA Langley Research Center [22]. A novel design method named Crossflow Attenuated NLF was used, which suppresses the TS and CF waves by carefully optimized airfoils, achieving a 6.8% drag reduction compared to the baseline CRM model. The transition experiments [23] were performed in the NTF wind tunnel at Langley Research Center. TSP images from the experiments are on the left side of Figure 11. In these images, brighter areas indicate the laminar region and darker areas indicate the turbulent. Turbulent wedges are seen due to the pressure orifices and surface imperfections. When compared to the computation, turbulent wedges should be neglected. A hybrid mesh with 25 million cells is generated in a manner similar to that for the DLR-F4 for computations listed in Table 1. Cells on the upper wing surface are 430×250×84 hexahedrons with a growth rate of 1.1 and a y^+ value of 0.5.

Table – 1 Flow conditions selected

Conditions	$\alpha(°)$	$Re_{MAC}(\times 10^6)$	Ma_∞	$Tu_\infty(\%)$
I	1.44848	14.979	0.85649	0.24
II	1.98031	14.946	0.85649	0.24

Skin friction distributions computed with the BCMcc model are demonstrated on the right side of Figure 11. The BCMcc model successfully predicts laminar flow. For both conditions, predicted transition fronts on the outboard wing are close to the experimental. The TSP images show the transition fronts rapidly jump from the upstream shock to the downstream one, and It is successfully reproduced by the BCMcc model. Transition fronts on the inboard wing are comparable to the experiment, but the wing root is predicted fully turbulent. Figure 12 shows the interaction between the turbulent boundary layer on the fuselage and the wing root, which makes the μ_t/μ exceeds 0.02 in front of the leading-edge, resulting in a turbulent flow with $\gamma_{BC} > 0.63$. This flow should be relaminarized by the favorable pressure gradient on the wing surface in real life [23]. However, the BCMcc model uses μ_t as its transport variable but the dissipative term for which does not take into account relaminarization. The μ_t is not dissipated enough on the wing surface and thus leads to a fully turbulent region.

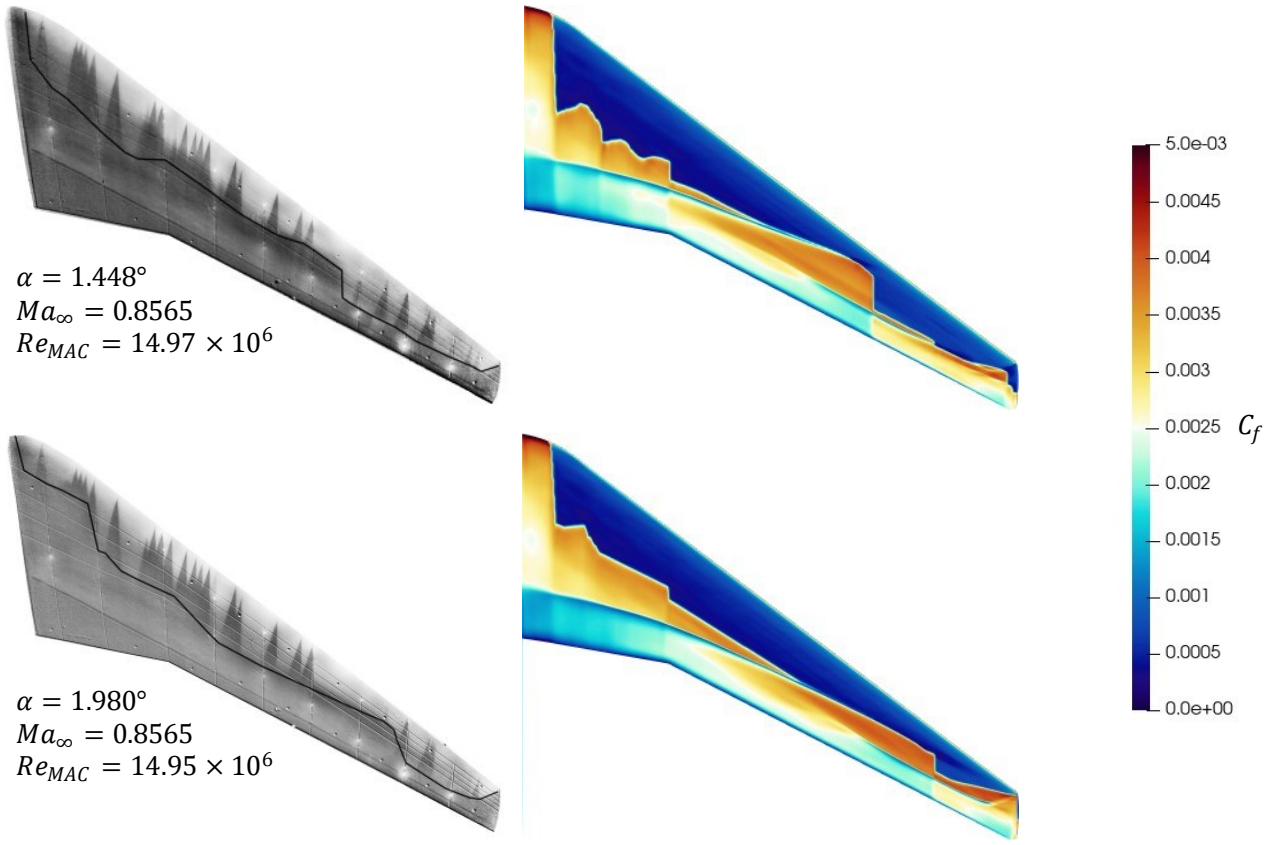

Figure 11 – TSP images (left) and skin friction coefficient calculated with BCMcc (right) on the CRM-NLF wing

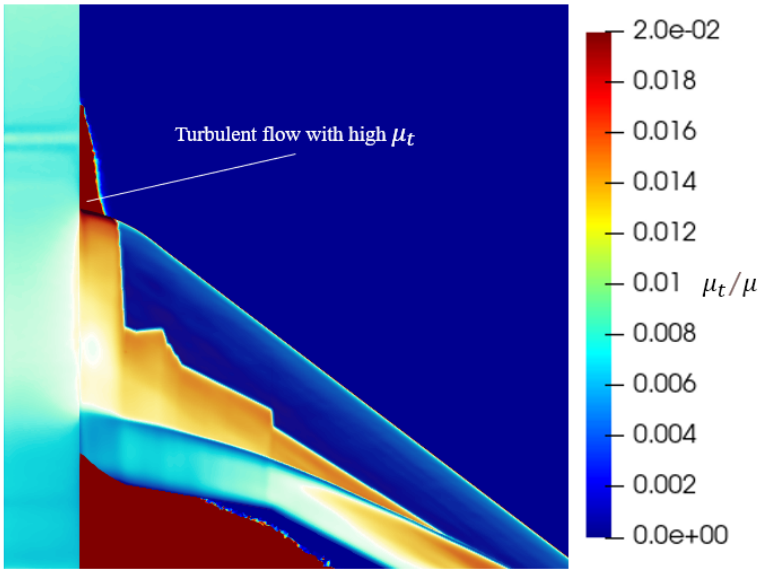

Figure 12 – Turbulent viscosity ratio near the CRM-NLF wing root

4. Conclusion

A newly proposed compressibility correction and an existing crossflow correction were integrated into the BCM model. The new model, referred to as BCMcc, was calibrated and validated, and compared with the original BCM and other popular LCTMs. The BCM model does not solve extra transport equations but uses an existing transported variable in the SA turbulence model. According to previous studies, the BCM model performs well at low speeds. However, we discover that it does not accurately predict transition fronts in transonic and crossflow cases.

The compressibility correction and the crossflow correction incorporated improved the performance under these conditions. The transition predicted by the BCMcc model on both the DLR-F4 and CRM-NLF aircraft is in good agreement with the corresponding experiments. But the lack of relaminarization effect caused a non-physical, fully turbulent wing root.

Besides, the γ-Re_θ model is found to handle TS transition reliably at transonic speed, but could not predict CF transition as expected. The results from the γ model in incompressible flow are good, but significantly differ from the experiment in compressible flow and the reason is yet to know.

To conclude, The BCMcc model performs decently in both low and high-speed flows and strong crossflows. As a simple algebraic LCTM, the BCMcc model could be useful in predicting transition for future transonic aircraft. Since the coefficients in the BCMcc model are few and meaningful, it could also be fine-tuned for other external Aerodynamic problems easily.

5. Acknowledgment

This work has been benefited greatly from the support of the Aeronautic Science Foundation of China under grant 2018ZA53014 and the Open Fund of Key Laboratory of Icing and Anti/De-icing of China under grant IADL20200101.

6. Contact Author Email Address

Please mail to Prof. Sangweimin: sangweimin@nwpu.edu.cn

7. Copyright Statement

References

[1] Beck N, Landa T, Seitz A, Boermans L, Liu Y and Radespiel R. Drag reduction by laminar flow control. *Energies*, Vol .11, No. 1, pp 1-28, 2018.

[2] Smith A M O and Gamberoni N. Transition, pressure gradient and stability theory. *Douglas Aircraft Company Report ES 26388*, 1956.

[3] Van Ingen J L. A suggested semi-empirical method for the calculation of the boundary layer transition region. *Technische Hogeschool Delft, Vliegtuigbouwkunde, Rapport VTH-74*, 1956.

[4] Langtry R B and Menter F R. Correlation-based transition modeling for unstructured parallelized computational fluid dynamics codes. *AIAA Journal*, Vol. 47, No. 12, pp 2894-2906, 2009.

[5] Menter F R, Langtry R B, Likki S R, Suzen YB, Huang PG and Volker S. A correlation-based transition model using local variables—part I: model formulation. *Journal of Turbomachinery*, Vol. 128, No. 3, pp 413-422, 2004.

[6] Menter F R, Smirnov P E, Liu T and Avancha R. A one-equation local correlation-based transition model. *Flow Turbulence Combust*, Vol. 95, No. 4, pp 583-619, 2015.

[7] Bas O, Cakmakcioglu S C, Kaynak U. A novel Intermittency distribution based transition model for low-re number airfoils. *Proc 31st AIAA Applied Aerodynamics Conference*, San Diego, pp 2531-2543, 2013.

[8] Mura R and Cakmakcioglu S C. A revised one-equation transitional model for external aerodynamics – part I: theory, validation and base cases. *Proc AIAA Aviation 2020 Forum*, Virtual, pp 2714, 2020.

[9] Cakmakcioglu S C, Bas O, Mura R and Kaynak U. A revised one-equation transitional model for External aerodynamics. *Proc AIAA Aviation 2020 Forum*, Virtual, pp 2706, 2020.

[10] Javadi A. Incorporating crossflow effects into the Spalart-Allmaras turbulent transition Model. *Proc 5th Thermal and Fluids Engineering Conference*, New Orleans, 2020.

[11] Wang S, Ge M, Deng X, Yu Q and Wang G. Blending of algebraic transition model and subgrid model for separated transitional flows[J]. *AIAA Journal*, Vol. 57, No. 11, pp 4684-4697, 2019.

[12] Nie S, Krimmelbein N, Krumbein A and Grabe C. Extension of a reynolds-stress-based transition transport model for crossflow transition. *Journal of Aircraft*, Vol. 55, No. 4, pp 1641-1654. 2018.

[13] Arnal D and Vermeersch O. Compressibility effects on laminar-turbulent boundary layer transition. *International Journal of Engineering Systems Modelling and Simulation*, Vol. 3, No. 1, pp 26-35, 2011.

[14] Van Driest E R, Blumer C B. Boundary layer transition-freestream turbulence and pressure gradient effects. *AIAA Journal*, Vol. 1, No. 6, pp 1303-1306, 1963.

[15] Fisher D F. In-flight transition measurement on a 10° cone at Mach numbers from 0.5 to 2.0. *NASA Technical Paper 1971*, 1982.

[16] Müller C and Herbst F. Modelling of crossflow-induced transition based on local variables. *Proc 6th European Conference on Computational Fluid Dynamics*, Barcelona, 2014.

[17] Arnal D, Habiballah M, Coustols E. Laminar instability theory and transition criteria in two and three-dimensional flow. *La Recherche Aerospatiale (English Edition)*, Vol. 2, pp 45-63, 1984.

[18] Langtry R B, Sengupta K, Yhe D T and Dorgan A J. Extending the γ-Re_θ local correlation-based transition model for crossflow effects. *Proc 45th AIAA Fluid Dynamics Conference*, Dallas, 2015.

[19] Economon T D, Palacios F, Copeland S R, Copeland S R, Lukaczyk T W and Alonso J J. SU2: An open-source suite for multiphysics simulation and design. AIAA Journal, Vol. 54, No. 3, pp 828-846, 2016.

[20] Kreplin H P, Vollmers H and Meier H. Wall shear stress measurements on an inclined prolate spheroid in the DFVLR 3m x 3m low-speed wind tunnel. *DFVLR-AVA*, 1985.

[21] Fey U, Engler R H, Egami Y, Iijima Y, Asai K, Jansen U and Quest J. Transition detection by temperature sensitive paint at cryogenic temperatures in the European Transonic Wind Tunnel (ETW). *Proc 20th International Congress on Instrumentation in Aerospace Simulation Facilities*, Göttingen, pp 77-88, 2003.

[22] Lynde M N and Campbell R L. Computational Design and Analysis of a Transonic Natural Laminar Flow Wing for a Wind Tunnel Model. *Proc 35th AIAA Applied Aerodynamics Conference*, pp 3058, 2017.

[23] Lynde M N, Campbell R L, Rivers M B, Viken S A, Chan D T and Watkins A N. Preliminary Results from an Experimental Assessment of a Natural Laminar Flow Design Method. *Proc AIAA Scitech 2019 Forum*, pp 2298, 2019.